

## Yamato 980459: Mineralogy and petrology of a new shergottite-related rock from Antarctica

Takashi Mikouchi<sup>1\*</sup>, Eisuke Koizumi<sup>1</sup>, Gordon McKay<sup>2</sup>, Akira Monkawa<sup>1</sup>,  
Yuji Ueda<sup>1</sup>, Jun Chokai<sup>1</sup> and Masamichi Miyamoto<sup>1</sup>

<sup>1</sup>*Department of Earth and Planetary Science, Graduate School of Science, University of Tokyo,  
7-3-1, Hongo, Bunkyo-ku, Tokyo 113-0033*

<sup>2</sup>*Mail Code SR, NASA Johnson Space Center, Houston, TX 77058, U.S.A.*

*\*Corresponding author. E-mail: mikouchi@eps.s.u-tokyo.ac.jp*

(Received March 11, 2004; Accepted June 17, 2004)

**Abstract:** Y980459, a new Martian meteorite from Antarctica, is composed of coarse porphyritic olivine grains (up to 2 mm) set in the groundmass of olivine and pyroxene with abundant glassy mesostasis containing dendritic olivine and pyroxene. The overall petrography of Y980459 is similar to those of olivine-phyric shergottites, but the absence of plagioclase and Ca phosphates makes Y980459 unique. Because of the absence of maskelynite, Y980459 is not a shergottite if we employ the classic definition of shergottite. Both olivine and pyroxenes are extensively zoned. The most magnesian olivine composition is Fo<sub>86</sub> and the olivine compositions are related to three different occurrence types of olivine (large phenocrysts, groundmass, and mesostasis). Pyroxenes have orthopyroxene cores (En<sub>81</sub>Fs<sub>17</sub>Wo<sub>2</sub>) mantled by pigeonite with the rims of augite. The mineralogy of Y980459 suggests that rapid crystallization of the parent magma caused significant undercooling and plagioclase did not nucleate. Probably, rapid transport of the Y980459 parent magma from the depth to the Martian surface crystallized olivine and pyroxene at first and eruption onto the surface quenched the magma producing the glassy mesostasis. Because olivine and pyroxene compositions of Y980459 are the most magnesian among Martian meteorites, Y980459 would represent one of the most primitive Martian magmas and derive from a highly reduced mantle. It seems that Y980459 contains no cumulus component, suggesting that Y980459 is a melt. In this sense, Y980459 is similar to QUE94201. The similarity in mineralogy and chemistry between Y980459 and olivine-phyric shergottites suggests derivation from a similar highly reduced mantle. However, Y980459 was the only sample that directly erupted onto the Martian surface without any accumulation processes.

**key words:** Mars, shergottite, olivine, pyroxene, undercooling

### 1. Introduction

Yamato 980459 (Y980459) is an 81-gram meteorite recovered from the bare ice field near the Minami-Yamato Nunataks, Antarctica during the 39th Japanese Antarctic Research Expedition program (Kojima *et al.*, 2000). A preliminary analysis of this meteorite (Kojima and Imae, 2002) shows that it is a new member of SNC (Shergottites-Nakhilites-Chassignite) meteorites that are widely accepted to have

originated from the planet Mars due to many pieces of evidence (*e.g.*, Bogard *et al.*, 1984; Pepin, 1985; McSween, 1994). As a result of the recent recovery of a number of meteorites from Antarctica and desert areas, the total number of Martian meteorites now reaches 30 (Meyer, 2003). Most of recently recovered Martian meteorites belong to a “shergottite” group. Although the shergottite group has been divided into two subgroups of “basaltic shergottites” and “lherzolic shergottites” based on petrology and mineralogy (*e.g.*, McSween, 1994), the recent recoveries of desert Martian meteorites have brought about recognition of another shergottite subgroup, “olivine-phyric shergottite” (*e.g.*, Goodrich, 2003). Olivine-phyric shergottites are characterized by the presence of large olivine grains set in the fine-grained basaltic groundmass of pyroxene and plagioclase (now shock-transformed to “maskelynite”). This type of rock has been important because recent Mars explorations have identified olivine at the surface of Mars, which is probably derived from olivine-bearing basalt (*e.g.*, Hoefen *et al.*, 2003). Furthermore, olivine-phyric shergottites can be key samples to understand petrogenetic relationships among different types of shergottites because olivine-phyric shergottites have several mineralogical similarities to both basaltic and lherzolic shergottites. The Y980459 meteorite is similar to olivine-phyric shergottites, but is clearly distinct in several respects (Dreibus *et al.*, 2003; Greshake *et al.*, 2003; Ikeda, 2003, 2004; Misawa, 2003, 2004; McKay and Mikouchi, 2003; Mikouchi *et al.*, 2003; Nagao and Okazaki, 2003; Okazaki and Nagao, 2004; Shih *et al.*, 2003; Shirai and Ebihara, 2003, 2004). Thus, the understanding of the formation of this new Martian meteorite will offer useful information to understand magmatic activity on Mars in general. In this paper, we report mineralogy and petrology of Y980459 as a part of the consortium study led by Dr. K. Misawa at National Institute of Polar Research (NIPR) (Misawa, 2003, 2004). Then, we discuss its possible crystallization history and mineralogical relationships to other Martian meteorites.

## 2. Samples and analytical techniques

We analyzed a polished thin section of Y980459 (Y980459,41-3) supplied from NIPR by the following methods after we carefully observed it by optical microscope. Backscattered electron (BSE) images were taken with a Hitachi S-4500 (field emission gun) scanning electron microscope with energy dispersive spectrometer (EDS) (Dept. of Earth and Planet. Science, University of Tokyo). X-ray elemental distribution maps were acquired by a JEOL JXA 8900L electron microprobe (Dept. of Earth and Planet. Science, University of Tokyo). Accelerating voltage was 15 kV, and the beam current was 60–80 nA. Modal abundances of minerals were calculated by combination of Si, Mg, Fe, Ca, Al, Ti, Na, and Cr X-ray maps of the  $8 \times 8$  mm area of the thin section. Quantitative wavelength dispersive analyses were performed on a JEOL Superprobe 733 electron microprobe (Ocean Research Institute, University of Tokyo) and a JEOL JCM 733 mk II microprobe (Dept. of Earth and Planet. Science, University of Tokyo) by using well-characterized natural and synthetic standards. Quantitative microprobe analyses of most phases were obtained at 15 kV accelerating voltage with a beam current of 12 nA. A defocused beam ( $10 \mu\text{m}$  in diameter) and lower probe current (8 nA) were employed for the analysis of glasses in the mesostasis and the magmatic inclusions to

minimize volatile loss (e.g., Mikouchi *et al.*, 1999). The mineral compositions of Y980459 were compared with those of other olivine-phyric shergottites using data from Mikouchi *et al.* (2001) (EETA79001 and Dar al Gani 476), and Mikouchi and Miyamoto (2002) (Dhofar 019).

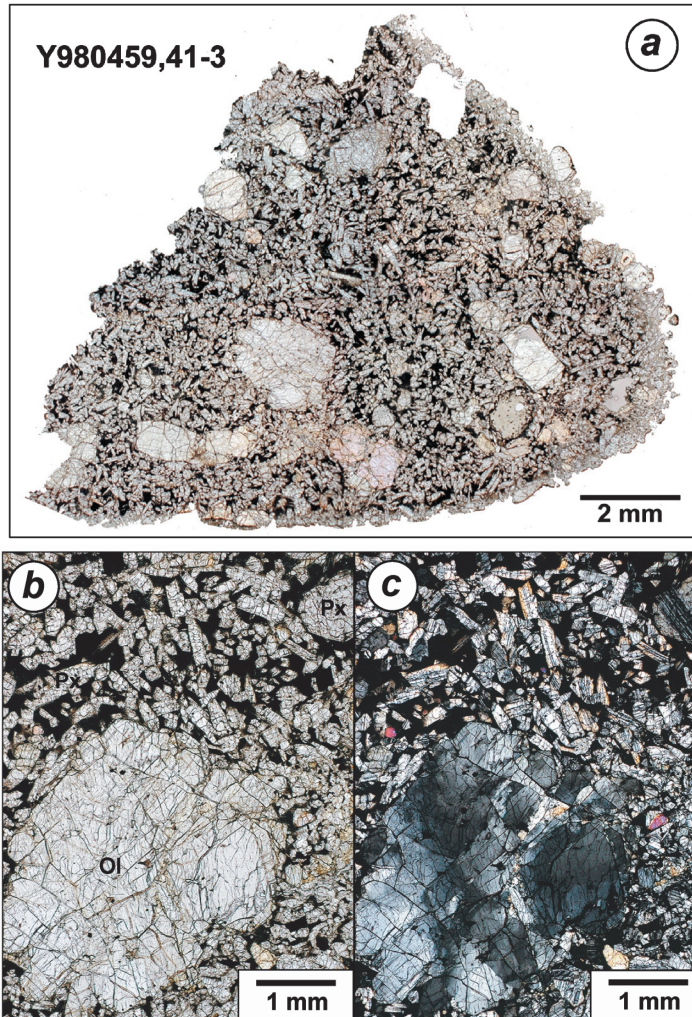


Fig. 1. (a) Optical photomicrograph (open nikol) of the Y980459 thin section (Y980459,41-3). Note the presence of coarse olivine phenocrysts reaching 2 mm in size and abundant dark mesostasis areas. (b) Optical photomicrograph (open nikol) of the largest olivine grain and the groundmass pyroxenes. Ol: olivine. Px: pyroxene. (c) Optical photomicrograph (crossed nikols) of the largest olivine grain and the groundmass pyroxenes corresponding to the same field of (b). Note the patchy extinction of the coarse olivine phenocryst and polysynthetic twinning of pyroxenes.

### 3. Petrography

Y980459,41-3 shows a porphyritic texture mainly composed of coarse olivine grains scattered in a fine-grained groundmass of pyroxene and olivine with abundant regions of the dark glassy mesostasis (Fig. 1). The modal abundances of minerals obtained by combination of several different elemental maps are 48% pyroxenes, 26% olivine, 25%

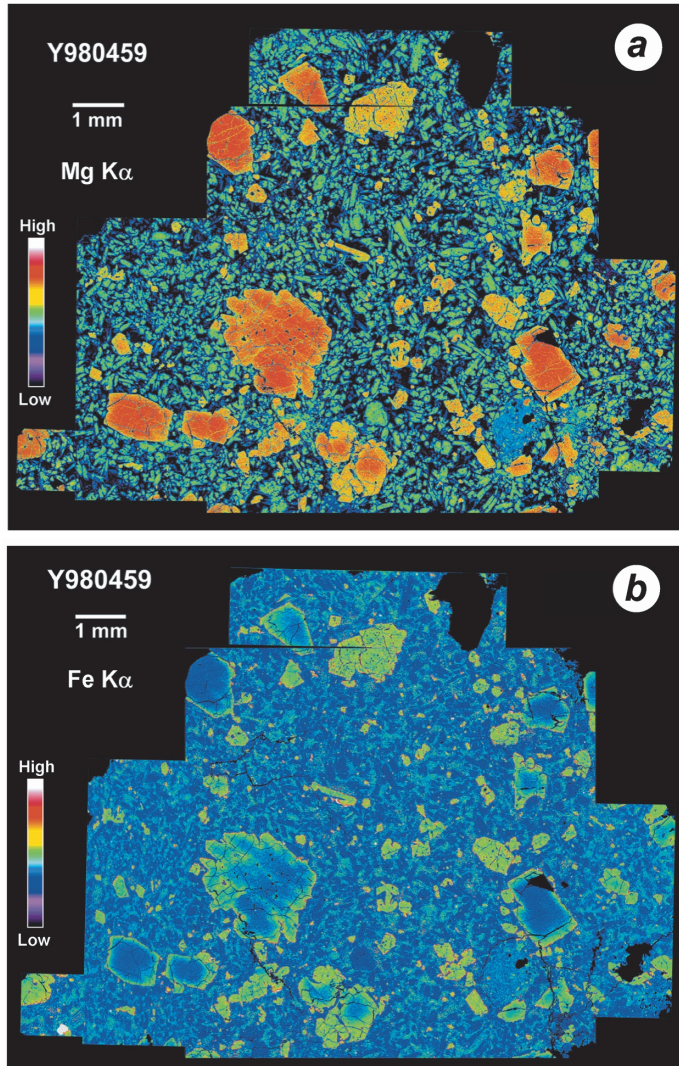


Fig. 2. (a) Mg X-ray map of Y980459. Olivine grains are colored from red to yellow due to the presence of chemical zoning. Pyroxenes are green in this map. (b) Fe X-ray map of Y980459. This map also indicates the presence of chemical zoning in olivine (grains showing the blue cores to the yellow rims). Olivine shows thin rimming of Fe-rich olivine (red) adjacent to the mesostasis. Also note the presence of small Fe-rich homogeneous olivine grains.

mesostasis and 1% other phases.

The coarse olivine phenocrysts reach up to 2 mm in size and show variable crystal shapes from nearly euhedral grains to anhedral grains (Figs. 1 and 2). These coarse olivines occur as individual single crystals rather than composite grains of a few crystals. Aside from these coarse olivine phenocrysts, there are smaller grains of olivine in the groundmass with sizes ranging from  $10\mu\text{m}$  to  $500\mu\text{m}$  (Figs. 2 and 3). These groundmass olivines also show variable grain shapes, but composite grains are common, unlike with the coarse olivine phenocrysts (Fig. 3). It is difficult to distinguish texturally these two types of olivine because there are olivine grains showing an intermediate size ( $\sim 1\text{mm}$ ). Some olivine grains contain abundant spherical glassy magmatic inclusions whose diameters are usually a few tens of  $\mu\text{m}$ , but some inclusions are present as irregular shapes (Fig. 4). There is a possibility that irregular-shaped inclusions are injection of the residual melt into the fractures of olivine. Magmatic inclusions are

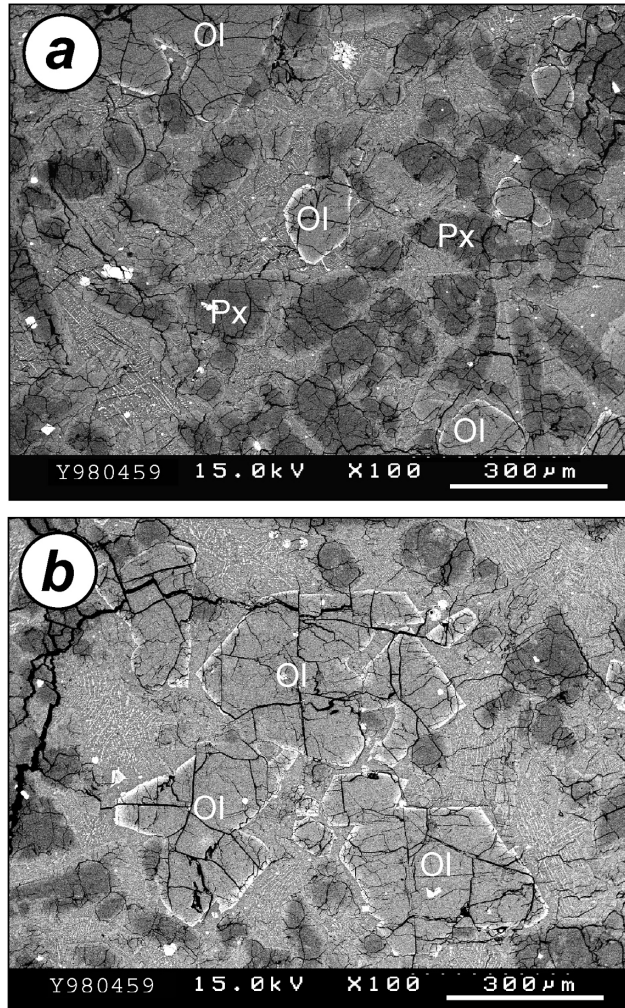


Fig. 3. BSE images showing the groundmass minerals in Y980459. (a) Note the presence of small olivine grains as large as pyroxenes. (b) Note the presence of composite olivine grains in the groundmass. Olivine is enriched in Fe where it is in contact with the mesostasis. Ol: olivine. Px: pyroxene.

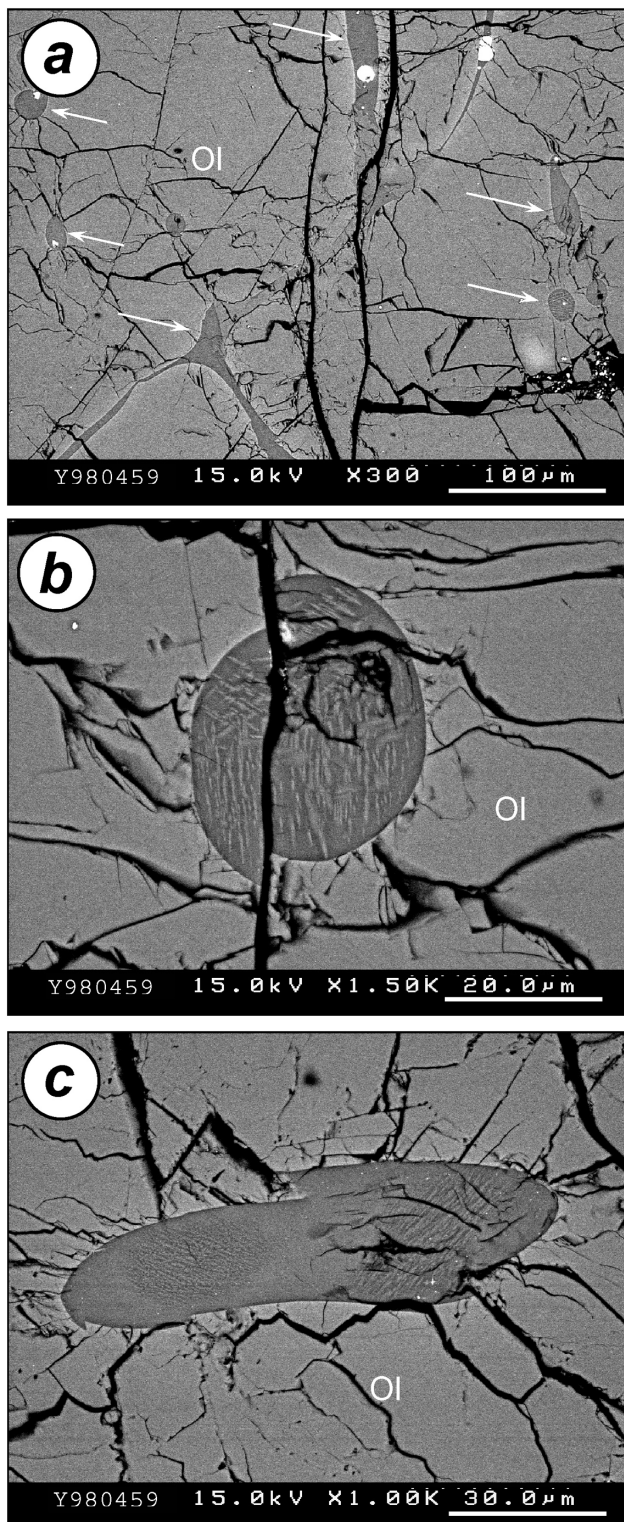


Fig. 4. BSE images showing the magmatic inclusions in olivines from Y980459. (a) This olivine contains abundant magmatic inclusions of two different shapes: spherical and irregular-shaped (indicated by arrows). (b) A rounded magmatic inclusion in olivine. This inclusion is faulted probably caused by shock. (c) An ovoid-shaped inclusion in olivine. This inclusion contains areas where crystallization of olivine and/or pyroxene started. Ol: olivine.

common in large olivine grains, but not all, and some small groundmass olivines contain magmatic inclusions. Thus, the abundance is quite heterogeneous. Chromite is sometimes enclosed in olivine. Many olivine grains show patchy or undulose extinction, probably due to a shock event (Fig. 1c).

Pyroxenes are present in the groundmass as prismatic euhedral to subhedral grains (Figs. 1, 2 and 3). In many cases, pyroxenes are interstitial to coarse olivine grains (Fig. 5). The maximum pyroxene size is  $\sim 500\mu\text{m}$ . Polysynthetic twinning is

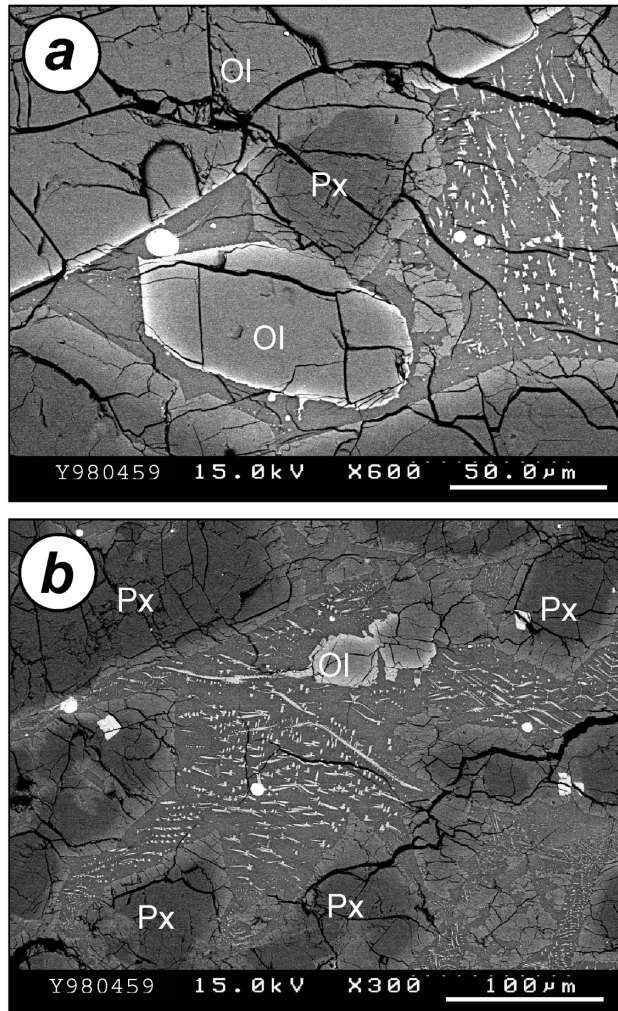


Fig. 5. BSE images showing the petrographic relation between the groundmass and the mesostasis in Y980459. (a) A pyroxene grain grows on the large olivine phenocryst. A small groundmass olivine is also present. Although olivine has thin Fe-rich rims adjacent to the mesostasis, the olivine-pyroxene boundaries do not show such Fe-enrichment. (b) The olivine grain located in the mesostasis shows a swallow-tail-like texture elongated into the mesostasis. Ol: olivine. Px: pyroxene.

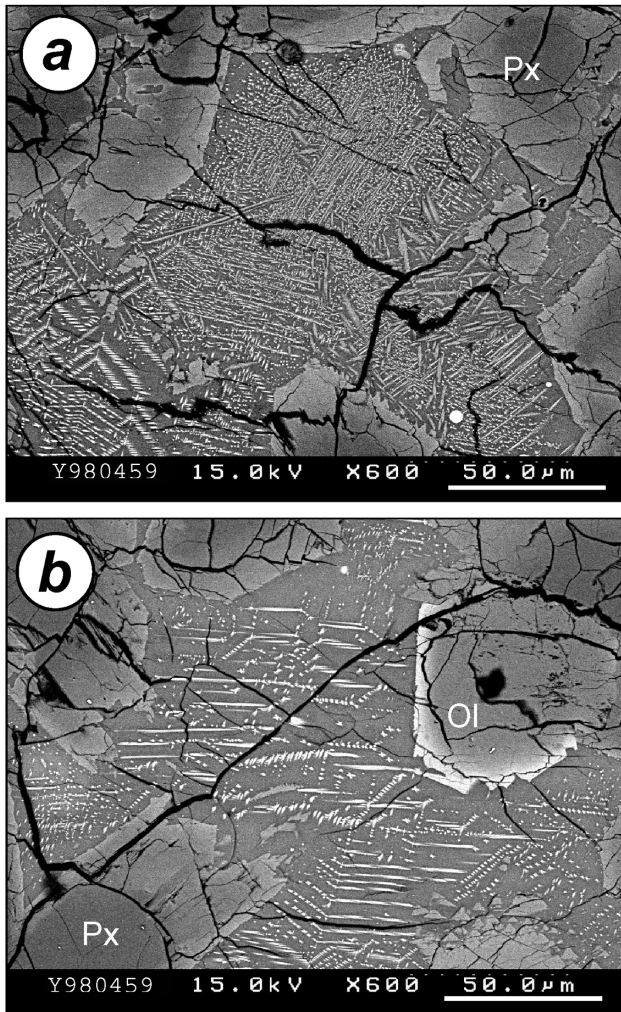


Fig. 6. BSE images showing heterogeneous crystallization of olivine and pyroxene in the mesostasis of Y980459. (a) In this mesostasis area, abundant pyroxenes crystallized, while olivine is rare. (b) In this mesostasis area, olivines are dominant. (c) Both olivine and pyroxene crystallized in this area in similar abundances. (d) The enlarged portion shown in (c). Pyroxenes (darker gray) are slightly larger than olivines (brighter gray). Px: pyroxene.

common in pyroxene probably due to shock as observed in other Martian meteorites (Fig. 1c). Magmatic inclusions are rare in pyroxene, unlike olivine.

The mesostasis areas are dark-colored and glassy (Fig. 1). They are interstitial to both olivine and pyroxene grains (Figs. 3 and 5). The mesostasis contains dendritic grains of olivine and pyroxene, which cause the mesostasis to appear opaque (Figs. 5 and 6). Some olivine grains in the mesostasis area are present as long blades reaching a few hundreds  $\mu\text{m}$  long. The distribution of olivine and pyroxene in the mesostasis is heterogeneous (Fig. 6). In some areas olivine is dominant, while in others pyroxene is. There are also areas where both olivine and pyroxene crystallized, and others where few if any crystals are present, although these areas are smaller than the previous three types of area. In many cases, pyroxene grew slightly larger than olivine in the mesostasis (Fig. 6). Except for these two major phases (olivine and pyroxene), other phases observed in the mesostasis are minor Fe sulfide spherules.

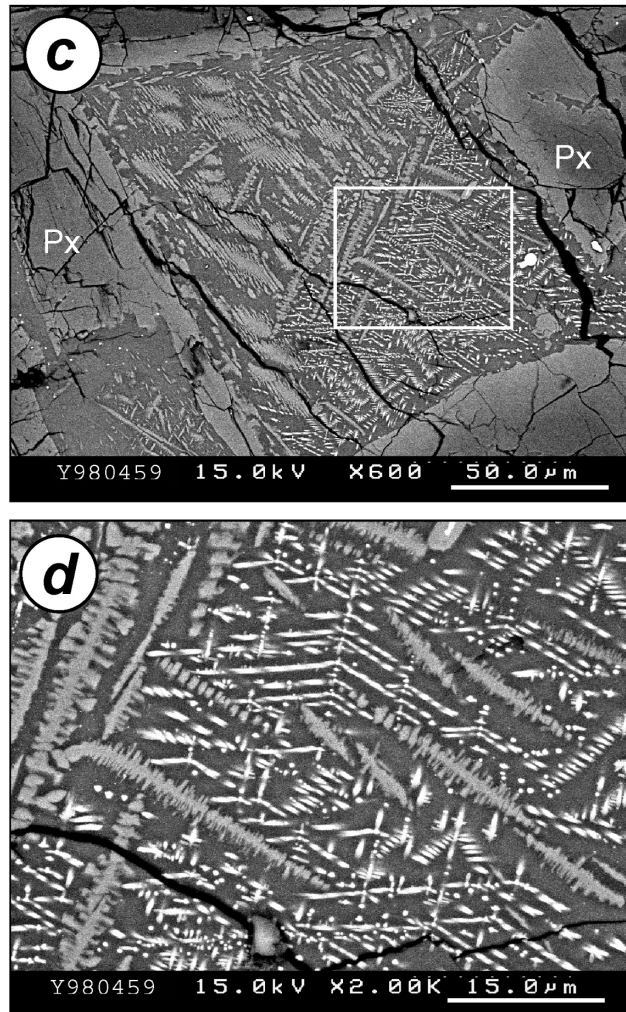


Fig. 6 (continued).

One of the most notable petrographic observations of Y980459 is that no plagioclase crystals were found, unlike in other Martian meteorites. Similarly, phosphates are absent in Y980459. The possible reason for the absence of these minerals is discussed in the following section.

The effect of shock metamorphism is moderate to extensive in Y980459 as suggested by the presence of undulose or patchy extinction of olivine and pyroxene (Fig. 1c). Rare shock melt pockets are present in the section studied (Fig. 7), but Greshake *et al.*, (2003) reported no shock melt in the section they examined. Because the shock melt pocket partially melted olivine and pyroxene in the mesostasis, the shock event clearly post-dated the final crystallization of Y980459. These observations are consistent with Greshake *et al.* (2003), which estimated the shock degree of Y980459 as 20–25 GPa.

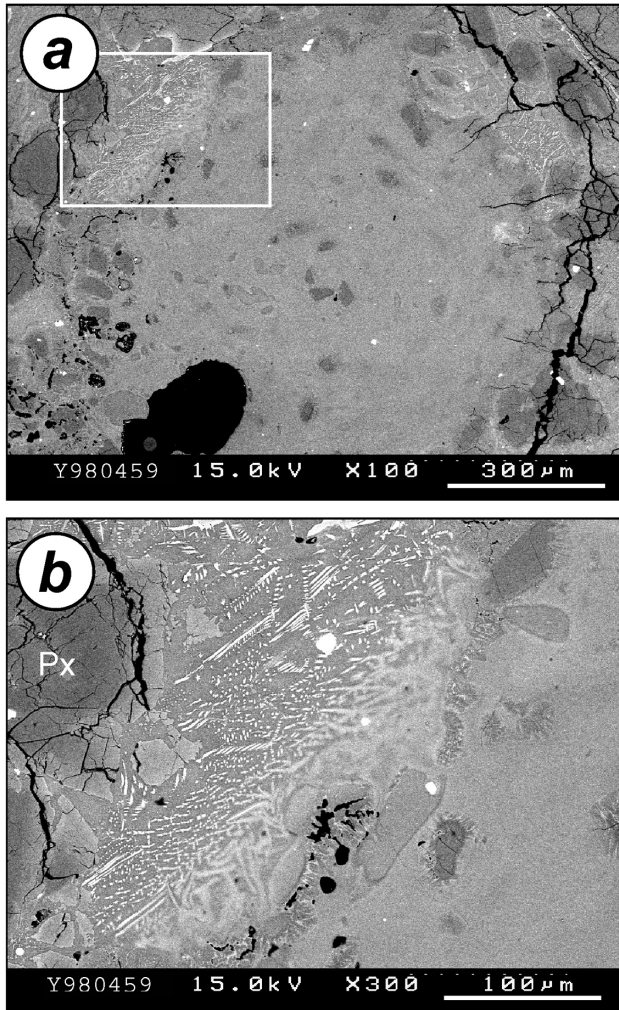


Fig. 7. BSE images of the shock melt pocket in Y980459. (a) The shock melt pocket has a heterogeneous composition with relict grains of pyroxene. (b) The enlarged portion shown in (a). Both olivine and pyroxene in the mesostasis partly melted at the contact to the shock melt pocket. Px: pyroxene.

## 4. Mineral chemistry

### 4.1. Olivine

Most olivine grains show extensive chemical zoning (Fig. 2). The zoning pattern is normal from the magnesian core to the ferroan rim in most large grains, but some grains show irregular zoning patterns. The compositional range of large olivine phenocrysts is  $Fo_{86-69}$  (Table 1, Fig. 8). Smaller olivine grains in the groundmass are more Fe-rich and most of them show irregular zoning patterns. The compositional range of these small olivine grains is  $Fo_{79-73}$ . There is thin rimming of Fe-rich olivine at the edge of all olivine grains adjacent to the mesostasis. Some parts of these rims show a swallow-tail-like texture elongated into the mesostasis (Fig. 5b). The chemical composition of these olivine rims is  $Fo_{73-40}$ . The dendritic olivine grains in the

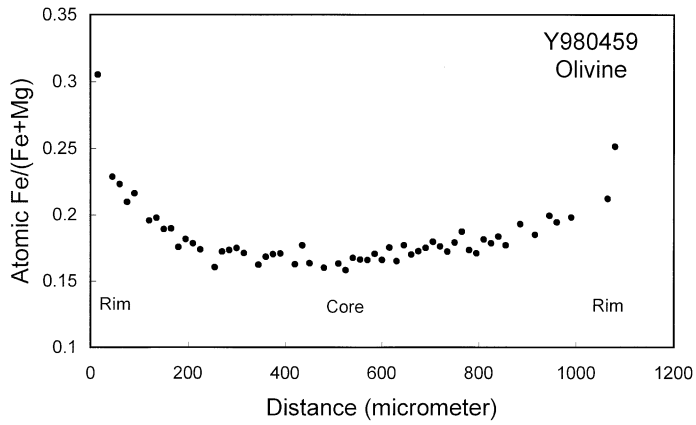


Fig. 8. The chemical zoning profile of the atomic  $Fe/(Fe+Mg)$  content (Fa content) of one of the coarse olivine phenocrysts in Y980459.

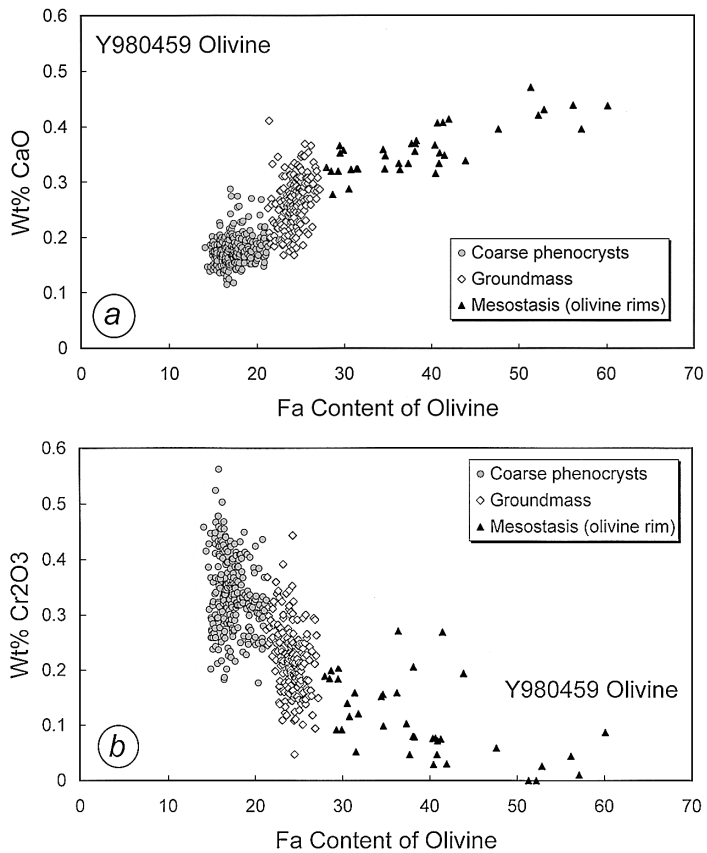


Fig. 9. (a) Variation of Fa and Ca contents of olivine in Y980459. (b) Variation of Fa and Cr contents of olivine in Y980459. Olivine compositions are clearly divided into three clusters and they correspond to three different types of olivine occurrences (coarse phenocryst, groundmass, and mesostasis).

mesostasis are too thin or small to be precisely analyzed by electron microprobe. However, the BSE images show nearly equal brightness to that of the olivine rims (Fig. 6), suggesting that they have similar compositions. Thus, there are three compositional clusters for olivine in Mg-Fe contents, corresponding to three occurrence of olivine: large phenocryst, groundmass, and mesostasis. Minor element contents of olivine also show similar behavior to the Fe-Mg contents (Fig. 9). The CaO contents in the coarse olivine phenocryst, groundmass olivine, and the mesostasis olivine are 0.15–0.2 wt%, 0.2–0.3 wt% and 0.3–0.4 wt%, respectively (Fig. 9a). Similarly, the Cr<sub>2</sub>O<sub>3</sub> contents are 0.45–0.2 wt%, 0.35–0.15 wt% and 0.15–0 wt%, respectively (Fig. 9b).

#### 4.2. Pyroxenes

Pyroxenes are also extensively zoned (Fig. 5, Table 1). The core is in the orthopyroxene compositional range (En<sub>80</sub>Fs<sub>18</sub>Wo<sub>2</sub>) and usually systematically zoned to the pigeonite composition (En<sub>70</sub>Fs<sub>23</sub>Wo<sub>7</sub>) (Figs. 10 and 11). Then, the rim is mantled by augite (En<sub>45</sub>Fs<sub>25</sub>Wo<sub>30</sub>) (Figs. 10 and 11). The pyroxene in the mesostasis is more Ca-, Fe-rich (En<sub>50</sub>Fs<sub>30</sub>Wo<sub>20</sub> to En<sub>25</sub>Fs<sub>40</sub>Wo<sub>35</sub>) and they are mostly augite. Some mesostasis pyroxenes were even more Fe-rich, up to En<sub>15</sub>Fs<sub>70</sub>Wo<sub>15</sub>. The Al and Ti contents monotonously increase both in low-Ca pyroxene (Wo<sub><25</sub>) and augite (Wo<sub>>25</sub>) as atomic Fe/(Fe+Mg) (*fe#*) increases (Figs. 12a and 12b). Al<sub>2</sub>O<sub>3</sub> and TiO<sub>2</sub> are particularly enriched in augite in the mesostasis, ranging from 4–9 wt% and 1–2 wt%, respectively. The Na content shows a similar behavior. The Na<sub>2</sub>O content is ~0.05 wt% in the orthopyroxene and it increases up to 0.3 wt% in mesostasis augite. In contrast, the Cr content shows different behavior because Cr is a compatible element, showing a decrease as the magma evolves (Fig. 12c). The Cr content of orthopyroxene is 0.3–0.8 wt% Cr<sub>2</sub>O<sub>3</sub>. Pigeonites have a slightly higher Cr content of up to 1.4 wt% Cr<sub>2</sub>O<sub>3</sub>, but augite is poor in Cr and the Cr<sub>2</sub>O<sub>3</sub> content is less than 0.5 wt%.

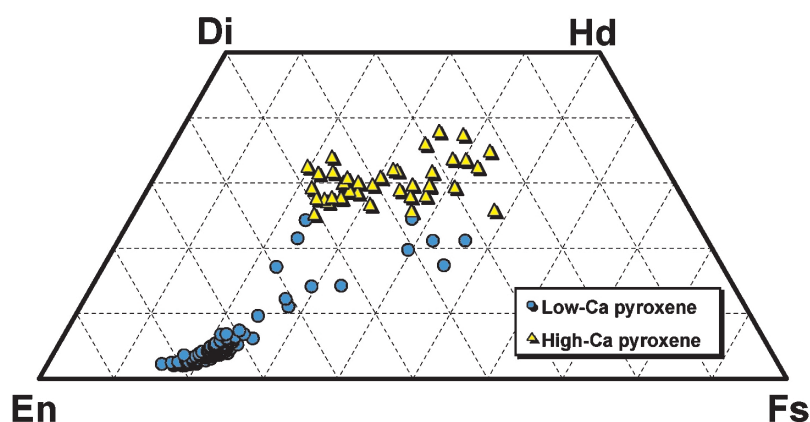


Fig. 10. Pyroxene quadrilateral of Y980459. Pyroxene in Y980459 shows systematic chemical zoning from orthopyroxene to pigeonite in the cores and the rims are augite. Low-Ca and high-Ca pyroxenes are defined by their wollastonite contents of lower than 25 and higher than 25, respectively.

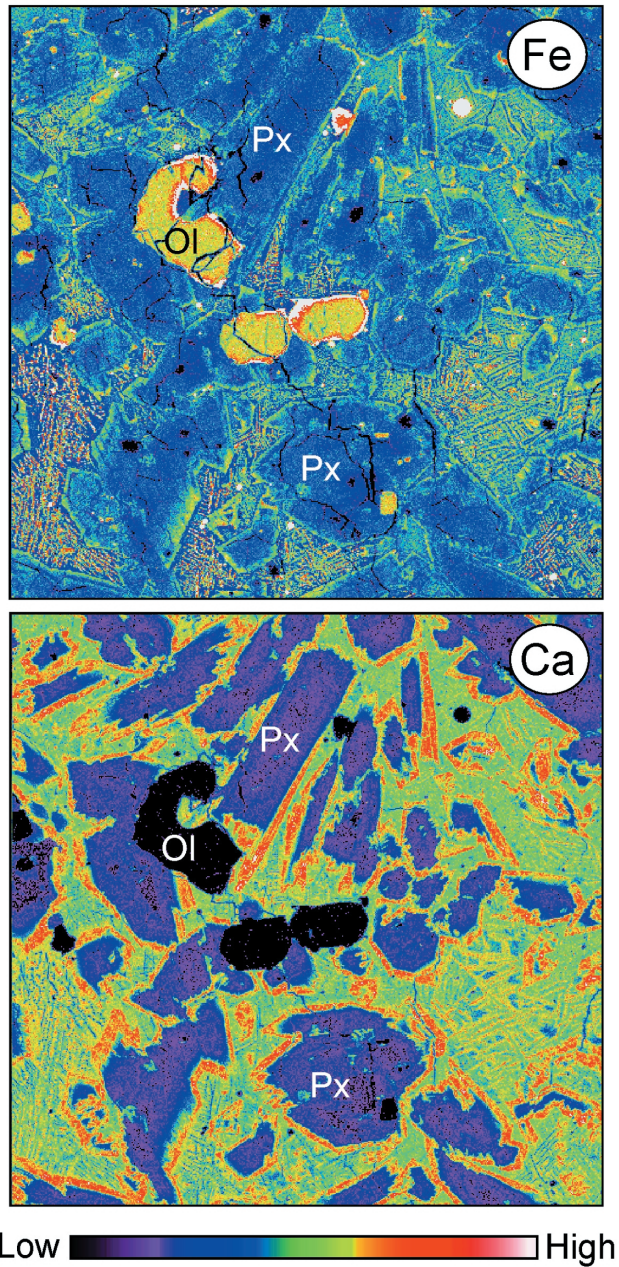


Fig. 11. Fe and Ca X-ray maps of Y980459. Pyroxenes have thin augite rims as the Ca map shows clear red-colored areas surrounding low-Ca pyroxene cores (purple to blue). The field of view is 1 mm. Ol: olivine. Px: pyroxene.

#### 4.3. Mesostasis and other phases

The mesostasis glass has a slightly heterogeneous composition depended upon crystallizing phases nearby. In the mesostasis where abundant olivine grains are present, the glass has 53 wt% SiO<sub>2</sub> and 17 wt% Al<sub>2</sub>O<sub>3</sub>, but the mesostasis with abundant pyroxene has a slightly lower Si (51 wt% SiO<sub>2</sub>) and Al (15 wt% Al<sub>2</sub>O<sub>3</sub>) glass composi-

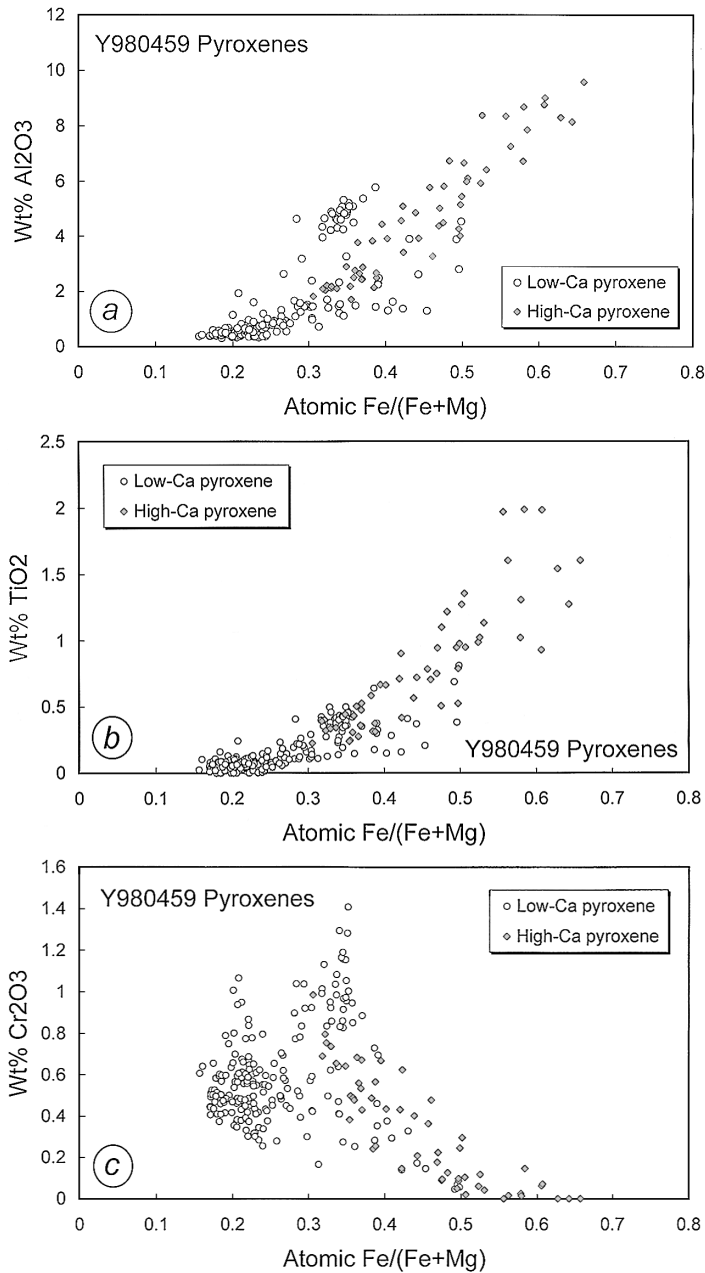


Fig. 12. (a) Al variation of pyroxenes in Y980459 versus the fe# variation. (b) Ti variation of pyroxenes in Y980459 versus the fe# variation. Both Al and Ti show monotonous increase as fe# increases. (c) Cr variation of pyroxenes in Y980459 versus the fe# variation. In contrast to Al and Ti, Cr shows a different behavior. Cr shows increase at around fe# of 0.35, but shows decrease as fe# increases. Low-Ca and high-Ca pyroxenes are defined by their wollastonite contents of lower than 25 and higher than 25, respectively as Fig. 10.

Table 1. Representative mineral compositions of major phases in Y980459.

	1	2	3	4	5	6	7	8	9
SiO <sub>2</sub>	39.51	39.27	38.30	38.26	33.39	56.02	53.41	50.70	45.14
Al <sub>2</sub> O <sub>3</sub>	0.04	0.02	0.03	0.05	0.04	0.50	0.89	2.35	8.35
TiO <sub>2</sub>	n.d.	n.d.	0.04	0.01	0.06	0.09	0.12	0.39	1.97
FeO	13.43	19.40	20.55	23.93	42.66	10.46	16.75	15.20	18.54
MnO	0.36	0.45	0.57	0.48	0.77	0.31	0.65	0.50	0.53
MgO	44.22	40.93	39.02	37.21	22.69	28.81	21.28	14.69	8.28
CaO	0.14	0.17	0.19	0.29	0.47	1.22	5.94	13.96	15.92
Na <sub>2</sub> O	0.01	n.d.	n.d.	n.d.	n.d.	0.02	0.04	0.11	0.20
K <sub>2</sub> O	0.02	0.02	0.02	0.02	n.d.	n.d.	0.01	0.01	n.d.
Cr <sub>2</sub> O <sub>3</sub>	0.39	0.32	0.18	0.12	n.d.	0.71	0.39	0.51	n.d.
V <sub>2</sub> O <sub>5</sub>	n.d.	n.d.	0.05	0.03	0.02	0.06	0.06	0.09	0.03
NiO	0.11	0.09	0.08	n.d.	n.d.	0.03	n.d.	0.09	0.02
P <sub>2</sub> O <sub>5</sub>	0.01	0.01	0.05	0.03	0.10	0.02	n.d.	0.15	0.70
Total	98.24	100.68	99.08	100.41	100.19	98.23	99.54	98.74	99.68
Fs						16.5	26.9	25.6	34.5
En						81.0	60.9	44.2	27.5
Wo						2.5	12.2	30.2	38.0
Fe#*	0.146	0.210	0.228	0.265	0.513	0.169	0.306	0.367	0.557

1. Coarse olivine phenocryst (core). 2. Coarse olivine phenocryst (rim). 3. Groundmass olivine (core). 4. Groundmass olivine (rim). 5. Fe-rich olivine rim. 6. Orthopyroxene core. 7. Pigeonite mantle. 8. Augite rim. 9. Fe-rich augite in the mesostasis. \*Fe# = Atomic Fe/(Fe+Mg). n.d. = not determined.

Table 2. Representative compositions of minor phases in Y980459.

	1	2	3	4	5	6
SiO <sub>2</sub>	0.81	53.80	51.03	60.72	48.68	50.65
Al <sub>2</sub> O <sub>3</sub>	8.53	17.58	14.72	11.11	6.28	7.03
TiO <sub>2</sub>	0.89	1.25	1.14	1.09	0.75	0.61
FeO	24.50	10.64	18.41	7.10	16.46	16.68
MnO	0.52	0.28	0.41	0.28	0.41	0.42
MgO	5.50	0.58	1.23	2.63	14.51	14.04
CaO	0.27	9.99	8.97	13.66	8.40	7.82
Na <sub>2</sub> O	n.d.	2.20	1.53	1.41	0.56	0.93
K <sub>2</sub> O	0.02	0.06	0.07	0.04	n.d.	0.03
Cr <sub>2</sub> O <sub>3</sub>	55.01	n.d.	0.01	0.13	0.63	0.26
V <sub>2</sub> O <sub>5</sub>	0.67	0.03	0.02	0.10	n.d.	0.03
NiO	n.d.	0.02	0.01	0.01	0.06	0.02
P <sub>2</sub> O <sub>5</sub>	n.d.	1.10	1.07	0.72	0.45	0.57
Total	96.72	97.54	98.63	99.00	97.19	99.09

1. Chromite. 2. Mesostasis glass (near olivine). 3. Mesostasis glass (near augite). 4. Glass in the magmatic inclusion in olivine. 5. Impact melt. 6. Fusion crust. n.d. = not determined.

tion (Table 2). In general, the mesostasis glass is enriched in P (1 wt%  $P_2O_5$ ) and alkali elements (2 wt%  $Na_2O$ ) (Table 2). The magmatic inclusion in olivine has a more Si-, Mg-rich (57–63 wt%  $SiO_2$  and 2–4 wt% MgO) and Al-, Fe-poor (11–12 wt%  $Al_2O_3$  and 6–8 wt% FeO) composition than the average mesostasis composition (Table 2).

Chromite in Y980459 is poor in Ti (up to 1 wt%  $TiO_2$ ) and its Al content has a range of 5–9 wt%  $Al_2O_3$  (Table 2). Fe sulfide in the mesostasis contains up to 2 wt% Ni.

We also analyzed fusion crust and impact melt in Y980459 (Table 2) and found that they are similar to the bulk composition of this meteorite reported by Misawa (2003).

### 5. Crystallization history of Y980459

The petrography and mineralogy of Y980459 suggest that a simple crystallization process can explain the formation of Y980459. We propose the following crystallization history for Y980459 (Fig. 13). Olivine and chromite crystallized from a parent melt. Probably, chromite crystallization was prior to olivine crystallization because chromites are usually enclosed in olivines. The estimated liquidus temperature of

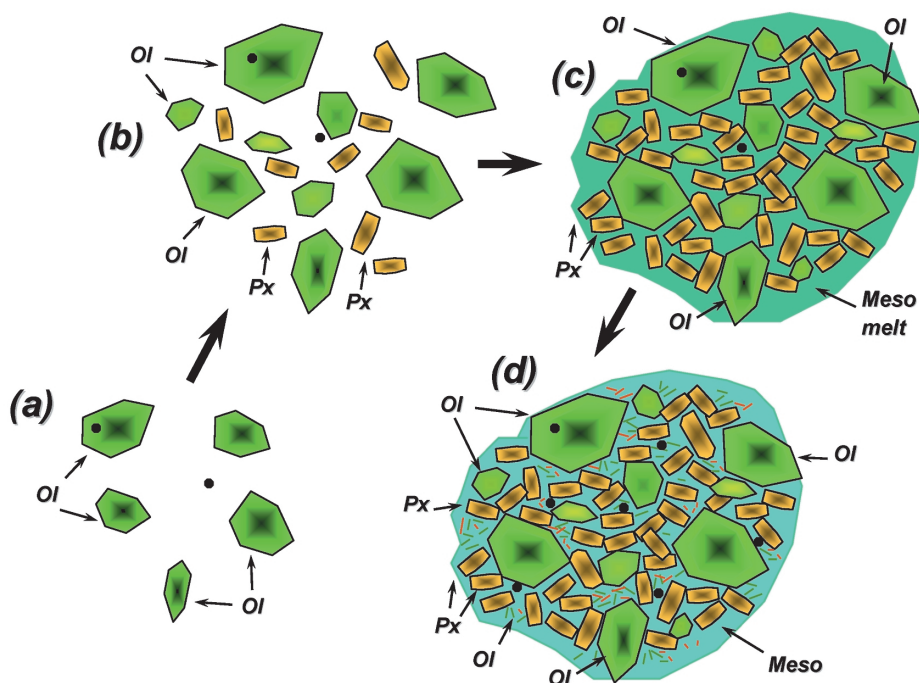


Fig. 13. Schematic illustration showing the formation history of Y980459. (a) Olivine crystallized from a magma probably with chromite. (b) Pyroxene started co-crystallization with olivine at some time. (c) Continuous crystallization of olivine and pyroxene trapped the interstitial melts. (d) Crystallization of dendritic olivine and pyroxene in the mesostasis. Ol: olivine. Px: pyroxene. Meso melt: interstitial mesostasis melt. Meso: mesostasis.

Y980459 is 1450°C (Koizumi *et al.*, 2004). As olivine continued crystallizing, some early phenocrysts became megacrysts. At some point, pyroxene started co-crystallizing with olivine. Koizumi *et al.* (2004) estimated that pyroxene started crystallizing with olivine at 1360°C using the MELTS software. We suggest that this point was marked by compositional kinks of Ca and Cr in olivine around Fo<sub>79</sub> (Fig. 9). The olivine in equilibrium with the most magnesian pyroxene ( $fe\# = 0.16$ ) is Fo<sub>80</sub> if we assume the  $kD^{fe\#}_{\text{olivine/low-Ca pyroxene}}$  of 1.24 which is employed from our crystallization experiments on shergottites. The obtained olivine composition is close to the groundmass olivine core composition (Fo<sub>79</sub>). This is also predicted in the calculation result by MELTS (Koizumi *et al.*, 2004). Then, the mesostasis minerals crystallized from a residual melt. Because the degree of undercooling was extremely significant, only olivine and pyroxene crystallized in the mesostasis and neither plagioclase nor Ca phosphates nucleated. The Al abundance in pyroxene monotonously increases (Fig. 12a), which suggests no crystallization of plagioclase unlike other shergottites (Fig. 14c) (*e.g.*, Mikouchi *et al.*, 1999). The pyroxene zoning sequence is from low-Ca pyroxene to high-Ca pyroxene and low-Ca pyroxene never crystallized again at late stages unlike other shergottites (*e.g.*, QUE94201) experiencing significant undercooling (Mikouchi *et al.*, 1998). This also suggests no crystallization of plagioclase. Thus, we believe that “coarse olivine phenocrysts” in Y980459 are true phenocrysts that crystallized from the parent melt of Y980459 having a similar composition to the bulk composition of this meteorite. This also means that Y980459 is a melt that contains neither xenocrystic nor cumulus components. The presence of abundant mesostasis area also suggests that an accumulation process was not significant.

Koizumi *et al.* (2004) and McKay *et al.* (2004) performed crystallization experiments using the bulk composition of Y980459 and they found that olivine crystallized as a liquidus phase and its composition (Fo<sub>83–84</sub>) is close to that measured in Y980459 (Fo<sub>86</sub>). Koizumi *et al.* (2004) also found that pyroxene compositions in their 2.5°C/hr cooling experiment nearly match with those in Y980459. Furthermore, the MELTS calculation result by Koizumi *et al.* (2004) is also consistent with those by crystallization experiments. Thus, these experimental results support the idea that Y980459 is a melt.

Another issue relating the crystallization of Y980459 is whether two-stage cooling history is necessary to grow large olivine under a slow cooling condition at first and then followed by fast cooling to form the glassy mesostasis. Greshake *et al.* (2003) and McKay *et al.* (2004) pointed out that some quenching process is necessary to produce a glassy mesostasis texture observed in Y980459. If this is the case, the possible scenario is that crystallization of olivine and groundmass grains occurred at depth and eruption onto the Martian surface caused quenching with the formation of the glassy mesostasis. However, extensive chemical zoning of olivine and pyroxene suggests that their crystallization started near the Martian surface. According to the cooling rate estimate for Dar al Gani 476 and EETA79001 olivines (Mikouchi *et al.*, 2001), Y980459 olivine would also crystallize at a similar cooling rate (0.03–5°C/hr). Thus, the burial depth of Y980459 at the time of initial olivine crystallization was up to 3 m. This will suggest that single rapid cooling history is responsible for the crystallization of Y980459. Because a single-stage crystallization process with fast cooling rate can form a porphy-

ritic or vitrophyric texture with glassy matrix (*e.g.*, Koizumi *et al.*, 2003), there is a possibility that Y980459 cooled rapidly from the beginning with a single-stage rapid cooling history. The presence of glassy magmatic inclusions in olivine phenocrysts also suggests rapid crystallization at the early stage of olivine crystallization. One of the possibilities to explain the cooling history of Y980459 is that rapid crystallization occurred during eruption from the depth to the Martian surface. The crystallization of olivine started during transport from the depth and final solidification occurred when the magma was at the Martian surface. Because a high liquidus temperature would promote crystallization of most phases of Y980459 at high temperatures, this may explain the quenching nature of this meteorite.

## 6. Relationship to other Martian meteorites

Y980459 is an unusual Martian meteorite in several respects. First of all, the absence of plagioclase and Ca phosphates is unique. This is the first shergottite meteorite that contains no plagioclase. However, texturally speaking, Y980459 is not a “shergottite” *sensu stricto*, because the classic definition of shergottite is a rock with pyroxene and maskelynitized plagioclase (Prior, 1920). From this point of view, Y980459 is more similar to nakhlites than shergottites because nakhlites are igneous rocks mainly composed of pyroxene and olivine (*e.g.*, McSween, 1994). However, olivine and pyroxene mineralogy of Y980459 clearly shows a closer relationship to shergottites than nakhlites. Except for the presence of the mesostasis, the overall mineralogy is especially similar to that of olivine-phyric shergottites. This is also supported by geochemical similarities in major and trace elements (Dreibus *et al.*, 2003; Shirai and Ebihara, 2003, 2004; Shih *et al.*, 2003). As discussed above, the absence of plagioclase is explained by the failure of nucleation due to the rapid cooling history of this meteorite. Thus, Y980459 probably experienced the fastest cooling rate among shergottites and is the first sample categorized into a new Martian meteorite group. If Y980459 had cooled more slowly, the crystallization of plagioclase would have occurred and overall texture could be similar to other olivine-phyric shergottites.

Another characteristic of Y980459 is its extremely magnesian composition. Such a magnesian composition of Y980459 shows that the parent magma of Y980459 had an exceptionally high liquidus temperature reaching nearly 1450°C (Koizumi *et al.*, 2004; McKay *et al.*, 2004). Combined with the rapid cooling history of this meteorite, it is unusual that such high magmatic temperature is accompanied with crystallization near the Martian surface. Thus, prompt transport of the magma from the depth to the Martian surface is required to achieve the formation of Y980459.

As more depleted samples are more reduced and less depleted samples are more oxidized among shergottites, trace element/isotopic signatures and the redox state of shergottites show a clear correlation (Wadhwa, 2001; Herd *et al.*, 2002). McKay *et al.* (2004) pointed out that crystallization of Y980459 occurred under reducing condition around  $\log f_{\text{O}_2} = \text{IW} + 1$  according to the spinel chemistry of this meteorite. Dreibus *et al.* (2003), Shirai and Ebihara (2004) and Shih *et al.* (2003) reported that Y980459 has a highly LREE-depleted pattern similar to other olivine-phyric shergottites, especially Dar al Gani 476 and Sayh al Uhaymir meteorites (Zipfel *et al.*, 2000; Wadhwa *et al.*,

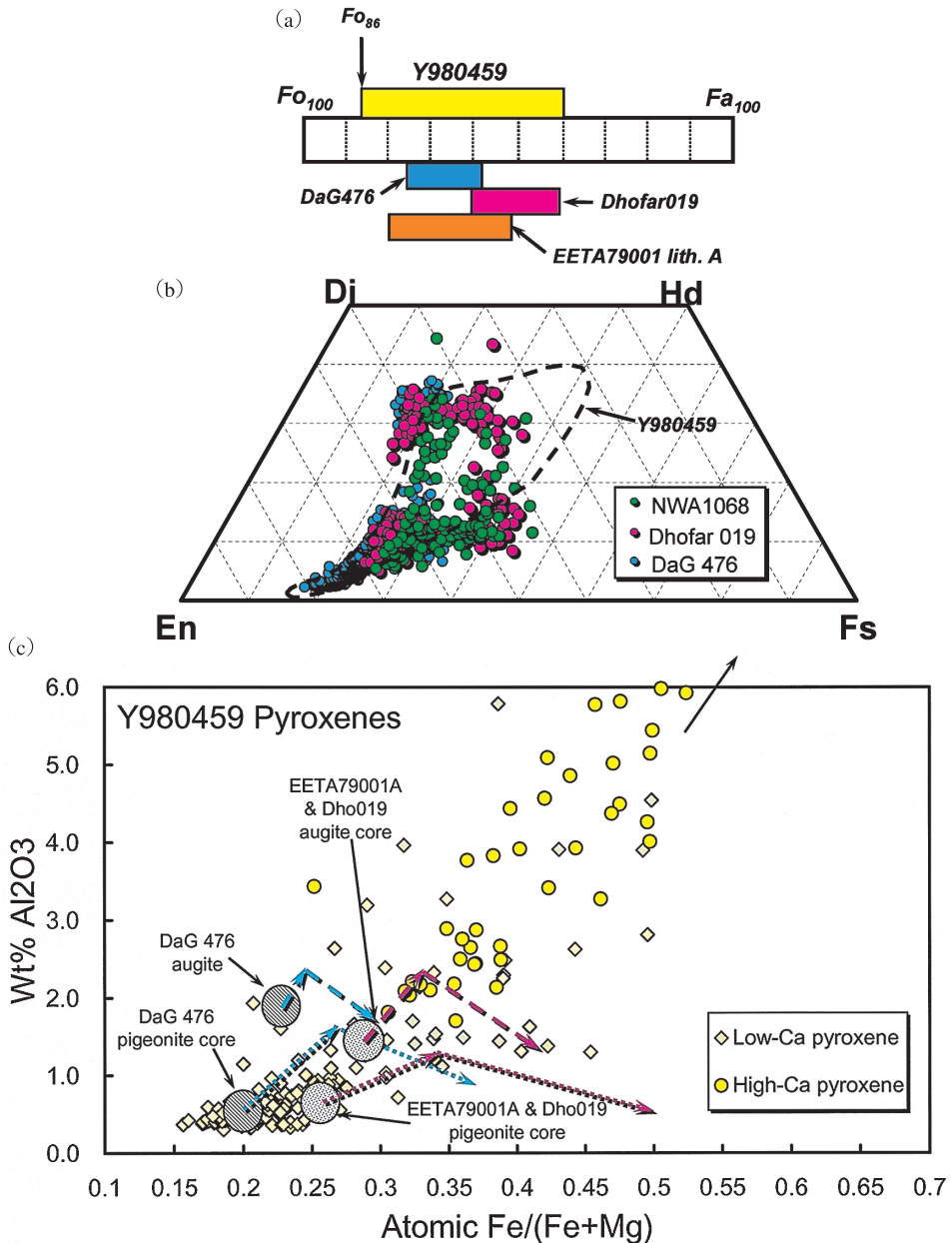


Fig. 14. (a) Olivine compositions of Y980459, Dar al Gani 476 (DaG476), Dhofar 019 and lithology A of EETA79001 (EETA79001 lith. A). (b) Pyroxene compositions of Northwest Africa 1068 (NWA1068), Dhofar 019, and DaG 476. The dotted area shows the composition of the Y980459 pyroxenes. (c) Fe# versus Al content of pyroxenes of Y980459 along with those from DaG 476, lithology A of EETA79001 (EETA79001A), and Dhofar 019. Unlike other olivine-phyric shergottites, no Al decrease is observed for Y980459 pyroxenes. Pyroxene compositions of EETA79001A are from phenocrysts grains in the groundmass. Y980459 has the most magnesian compositions for both olivine and pyroxene.

2001; Goodrich, 2003). Thus, Y980459 is a depleted sample formed under reducing condition, matching with the above correlations. Y980459 probably represents one of the most primitive Martian magmas and would derive from a highly reduced mantle (Borg *et al.*, 1997; Herd *et al.*, 2002).

The mineral compositions of olivine and pyroxene are generally similar to those of olivine-phyric shergottites (Fig. 14), which is consistent with the depleted chemistry of this meteorite (Dreibus *et al.*, 2003; Shirai and Ebihara, 2004; Shih *et al.*, 2003). However, Y980459 has more Mg-rich core compositions for both olivine ( $\text{Fo}_{86}$ ) and pyroxene ( $\text{En}_{81}\text{Fs}_{17}\text{Wo}_2$ ) (Fig. 14). Thus, Y980459 is the most magnesian Martian meteorite so far found. Y980459 appears to be a rock that directly crystallized from the magma without any accumulation processes, which is in contrast to other olivine-phyric shergottites that are cumulate rocks (*e.g.*, Mikouchi *et al.*, 2001). Although Y980459 and olivine-phyric shergottites derived from a similar highly reduced mantle, only Y980459 directly erupted onto the Martian surface without any accumulation processes. In contrast, other olivine-phyric shergottites experienced accumulation processes at some points during their crystallization. In this sense, Y980459 is similar to QUE94201, which is a sample directly crystallized from the magma without accumulation (*e.g.*, Mikouchi *et al.*, 1998). QUE94201 is similar to Y980459 in that it is a depleted sample formed under reducing condition. Because these two meteorites have similar crystallization ages around 300 Ma (Borg *et al.*, 1997; Shih *et al.*, 2004), they may represent a contemporary igneous event on Mars. In fact, their ejection ages are also similar (2.1–2.8 Ma) (Eugster *et al.*, 2002; Nagao and Okazaki, 2003; Okazaki and Nagao, 2004).

## 7. Conclusions

Y980459 is a new martian meteorite showing several mineralogical similarities to olivine-phyric shergottites. However, there are clear differences between them. The two most significant characteristics of Y980459 are the absence of plagioclase and highly magnesian mineral compositions. Y980459 is the first shergottite that contains no late-crystallization phases including plagioclase. The rapid crystallization of Y980459 parent magma caused significant undercooling of the magma, which brought about failure of plagioclase nucleation. The most plausible scenario for the formation of Y980459 is that rapid transport of the Y980459 parent magma from the depth to the Martian surface crystallized olivine and pyroxene and eruption onto the surface quenched the magma producing the glassy mesostasis. The olivine and pyroxene compositions of Y980459 are the most magnesian among Martian meteorites. Thus, Y980459 is the most primitive Martian meteorite. It seems that Y980459 contains no cumulus component, suggesting that Y980459 is a melt as supported by experimental results by Koizumi *et al.* (2004) and McKay *et al.* (2004). Because Y980459 has characteristics of depleted chemistry, it probably represents one of the most primitive Martian magmas and would derive from a highly reduced mantle. Although Y980459 and olivine-phyric shergottites derived from a similar highly reduced mantle, Y980459 was the only sample that directly erupted onto the Martian surface without any accumulation processes. In this sense, Y980459 is similar to QUE94201 as they are

depleted samples formed under reducing condition.

### Acknowledgments

The Y980459 sample was kindly allocated by NIPR as a part of the consortium study led by Dr. K. Misawa (Misawa, 2003, 2004). We thank Drs. K. Misawa, A. Yamaguchi, N. Imae, and P. Buchanan for useful discussions. We also thank Mr. O. Tachikawa and Mr. H. Yoshida for their technical assistance during electron beam analyses. Comprehensive and constructive reviews by Dr. Y. Ikeda and an anonymous reviewer improved the quality of the manuscript. The electron microscopy was performed in the Electron Microbeam Analysis Facility for mineralogy at Dept. of Earth and Planetary Science, University of Tokyo.

### References

- Bogard, D.D., Nyquist, L.E. and Johnson, P. (1984): Noble gas contents of shergottites and implications for the Martian origin of SNC meteorites. *Geochim. Cosmochim. Acta*, **48**, 1723–1739.
- Borg, L.E., Nyquist, L.E., Taylor, L.A., Wiesmann, H. and Shih, C.-Y. (1997): Constraints on Martian differentiation processes from Rb-Sr and Sm-Nd isotopic analyses of the basaltic shergottite QUE 94201. *Geochim. Cosmochim. Acta*, **61**, 4915–4931.
- Dreibus, G., Haubold, R., Huisl, W. and Spettel, B. (2003): Comparison of the chemistry of Yamato 980459 with DaG 476 and SaU 005. *International Symposium—Evolution of Solar System Materials: A New Perspective from Antarctic Meteorites*. Tokyo, Natl Inst. Polar Res., 19–20.
- Eugster, O., Busemann, H., Lorenzetti, S. and Terribilini, D. (2002): Ejection ages from  $^{81}\text{Kr}$ - $^{83}\text{Kr}$  dating and pre-atmospheric sizes of Martian meteorites. *Meteorit. Planet. Sci.*, **37**, 1345–1360.
- Goodrich, C.A. (2003): Petrogenesis of olivine-phyric shergottites Sayh al Uhaymir 005 and Elephant Moraine A79001 lithology A. *Geochim. Cosmochim. Acta*, **67**, 3735–3772.
- Greshake, A., Fritz, J. and Stöffler, D. (2003): Petrography and shock metamorphism of the unique shergottite Yamato 980459. *International Symposium—Evolution of Solar System Materials: A New Perspective from Antarctic Meteorites*. Tokyo, Natl Inst. Polar Res., 29–30.
- Herd, C.D.K., Borg, L.E., Jones, J.H. and Papike, J.J. (2002): Oxygen fugacity and geochemical variations in the Martian basalts: Implications for Martian basalt petrogenesis and the oxidation state of the upper mantle of Mars. *Geochim. Cosmochim. Acta*, **66**, 2025–2036.
- Hoefen, T.M., Clark, R.N., Bandfield, J.L., Smith, M.D., Pearl, J.C. and Christensen, P.R. (2003): Discovery of olivine in the Nili Fossae region of Mars. *Science*, **302**, 627–630.
- Ikeda, Y. (2003): Petrology of the Yamato 980459 shergottite. *International Symposium Evolution of Solar System Materials: A New Perspective from Antarctic Meteorites*. Tokyo, Natl Inst. Polar Res., 42.
- Ikeda, Y. (2004): Petrology of the Yamato 980459 shergottite. *Antarct. Meteorite Res.*, **17**, 35–54.
- Kojima, H. and Imae, N. (2002): Y980459. *Meteorite Newslett.*, **11** (1), 48.
- Kojima, H., Kaiden, H. and Yada, T. (2000): Meteorite search by JARE-39 in 1998–1999 season. *Antarct. Meteorite Res.*, **13**, 1–8.
- Koizumi, E., Mikouchi, T., McKay, G., Monkawa, A., Le, L. and Miyamoto, M. (2003): Implication for the slow linear cooling origin of vitrophyric textures in basaltic rocks. *Meteorit. Planet. Sci.*, **38**, A94.
- Koizumi, E., Mikouchi, T., McKay, G., Monkawa, A., Chokai, J. and Miyamoto, M. (2004): Yamato 980459: Crystallization of martian magnesian magma. *Lunar and Planetary Science XXXV*. Houston, Lunar Planet. Inst., Abstract #1494 (CD-ROM).
- McKay, G. and Mikouchi, T. (2003): Crystallization of Antarctic shergottite Yamato 980459. *International Symposium—Evolution of Solar System Materials: A New Perspective from Antarctic Meteorites*. Tokyo, Natl Inst. Polar Res., 76–77.
- McKay, G., Le, L., Schwandt, C., Mikouchi, T., Koizumi, E. and Jones, J. (2004) Yamato 980459: The most

- primitive shergottite? Lunar and Planetary Science XXXV. Houston, Lunar Planet. Inst., Abstract #2154 (CD-ROM).
- McSween, H.Y., Jr. (1994): What we have learned about Mars from SNC meteorites. *Meteoritics*, **29**, 757–779.
- Meyer, C. (2003): Mars Meteorite Compendium - 2003. NASA Johnson Space Center, Houston, Texas, USA, (<http://www-curator.jsc.nasa.gov/curator/antmet/mmc/mmc.htm>).
- Mikouchi, T. and Miyamoto, M. (2002): Mineralogy and olivine cooling rates of the Dhofar 019 shergottite. *Antarct. Meteorite Res.*, **15**, 122–142.
- Mikouchi, T., Miyamoto, M. and McKay, G. (1998): Mineralogy of Antarctic basaltic shergottite Queen Alexandra Range 94201: Similarities to Elephant Moraine A79001 (Lithology B) martian meteorite. *Meteorit. Planet. Sci.*, **33**, 181–189.
- Mikouchi, T., Miyamoto, M. and McKay, G. (1999): The role of undercooling in producing igneous zoning trends in pyroxenes and maskelynites among basaltic Martian meteorites. *Earth. Planet. Sci. Lett.*, **173**, 235–256.
- Mikouchi, T., Miyamoto, M. and McKay, G. (2001): Mineralogy and petrology of the Dar al Gani martian meteorite: Implications for its cooling history and relationship to other shergottites. *Meteorit. Planet. Sci.*, **36**, 531–548.
- Mikouchi, T., Koizumi, E., McKay, G., Monkawa, A., Ueda, Y. and Miyamoto, M. (2003): Mineralogy and petrology of the Yamato 980459 martian meteorite: A new shergottite-related rock. *International Symposium—Evolution of Solar System Materials: A New Perspective from Antarctic Meteorites*. Tokyo, Natl Inst. Polar Res., 82–83.
- Misawa, K. (2003): The Yamato 980459 shergottite consortium. *International Symposium Evolution of Solar System Materials: A New Perspective from Antarctic Meteorites*. Tokyo, Natl Inst. Polar Res., 84–85.
- Misawa, K. (2004): The Yamato 980459 olivine-phyric shergottite consortium. *Antarct. Meteorite Res.*, **17**, 1–12.
- Nagao, K. and Okazaki, R. (2003): Noble gases of Y980459 shergottite. *International Symposium—Evolution of Solar System Materials: A New Perspective from Antarctic Meteorites*. Tokyo, Natl. Inst. Polar Res., 94.
- Okazaki, R. and Nagao, K. (2004): Noble gases of Yamato 980459 shergottite. *Antarct. Meteorite Res.*, **17**, 68–83.
- Pepin, R.O. (1985): Evidence of martian origins. *Nature*, **317**, 473–475.
- Prior, G.T. (1920): The classification of meteorites. *Mineral. Mag.*, **19**, 51–63.
- Shih, C.-Y., Nyquist, L.E. and Wiesmann, H. (2003): Isotopic studies of Antarctic olivine-phyric shergottite Y980459. *International Symposium—Evolution of Solar System Materials: A New Perspective from Antarctic Meteorites*. Tokyo, Natl Inst. Polar Res., 125–126.
- Shirai, N. and Ebihara, M. (2003): Chemical composition of Yamato 980459. *International Symposium—Evolution of Solar System Materials: A New Perspective from Antarctic Meteorites*. Tokyo, Natl Inst. Polar Res., 127–128.
- Shirai, N. and Ebihara, M. (2004): Chemical characteristics of a Martian meteorite, Yamato 980459. *Antarct. Meteorite Res.*, **17**, 55–67.
- Wadhwa, M. (2001): Redox state of Mars' upper mantle and crust from Eu anomalies in shergottite pyroxenes. *Science*, **291**, 1527–1530.
- Wadhwa, M., Lentz, R.C.F., McSween, H.Y., Jr. and Crozaz, G. (2001): A petrologic and trace element study of Dar al Gani 476 and Dar al Gani 489: Twin meteorites with affinities to basaltic and lherzolithic shergottites. *Meteorit. Planet. Sci.*, **36**, 195–208.
- Zipfel, J., Scherer, P., Spettel, B., Dreibus, G. and Schultz, L. (2000): Petrology and chemistry of the new shergottite Dar al Gani 476. *Meteorit. Planet. Sci.*, **35**, 95–106.